Journal of Alloys and Compounds 507 (2010) L4–L7

Contents lists available at ScienceDirect

Journal of Alloys and Compounds

journal homepage: www.elsevier.com/locate/jallcom

Letter

Multiferroic behavior and electrical conduction of $BiFeO_3$ thin film deposited on quartz substrate

Jiagang Wu, John Wang*

Department of Materials Science and Engineering, Faculty of Engineering, National University of Singapore, 117574 Singapore, Singapore

ARTICLE INFO

Article history:
Received 5 July 2010
Received in revised form 15 July 2010
Accepted 17 July 2010
Available online 30 July 2010

Keywords:
$BiFeO_3$ thin films
Quartz substrate
Multiferroic properties
Impedance study

ABSTRACT

Multiferroic $BiFeO_3$ thin films were deposited on $SrRuO_3$-buffered quartz substrates by off-axis radio frequency magnetron sputtering. The $BiFeO_3$ thin film exhibits the desired multiferroic behavior ($2P_r \sim 97.41\ \mu C/cm^2$ and $2M_s \sim 10.3$ emu/cm^3). On the basis of the temperature- and frequency-dependent impedance studies, oxygen vacancies are shown to be responsible for the dielectric relaxation and conduction in the $BiFeO_3$ thin film, where the scaling behavior of imaginary part of the electric modulus suggests that the relaxation mechanism does not change over the temperature range investigated.

1. Introduction

Multiferroic $BiFeO_3$ (BFO) possesses a giant remanent polarization, a room-temperature magnetization, and a high Curie temperature ($T_c = 1103$ K) [1–3], promising as a candidate material for a high-density ferroelectric random access memory and several other technologically demanding applications [1–3]. However, its large leakage current hinders the potentially feasible applications that have been considered for the BFO thin films [2,3].

Several different attempts have been made to reduce the leakage current for BFO thin films, for example, by the use of an single crystal substrate [4,5], an appropriate buffer layer [6–9], construction of a multilayer structure [10–12], and ion substitutions for Bi and/or Fe [6,13,14]. In the past, single crystal substrates and silicon substrates have been widely used to deposit BFO thin films [4–7,11,12], where the ferroelectric behavior are strongly affected by the type of substrates [13]. It is thus rather difficult to characterize the intrinsic behavior of BFO thin films. Although quartz is a widely used substrate material, there have been few reports on the multiferroic behavior and electrical conduction of BFO thin films deposited on the quartz substrate with a $SrRuO_3$ (SRO) buffer layer. Therefore, we focused on the electrical properties and physical mechanism of BFO thin films deposited on the quartz substrates.

In this work, the BFO thin film was *in situ* deposited on the SRO-buffered quartz substrate by off-axis radio frequency (rf) sputtering, where the multiferroic behavior and electrical conduction were investigated. Desired multiferroic behavior is clearly observed for the BFO thin film. Oxygen vacancies are involved in the dielectric relaxation and conduction, as demonstrated by the temperature- and frequency-dependent impedances.

2. Experimental procedures

The BFO thin film was deposited on the quartz substrate by off-axis rf sputtering with a SRO buffer layer. The two-inch BFO ceramic target was synthesized by solid state reaction of the mixed oxides of Fe_2O_3 and Bi_2O_3 with 20 mol% excess Bi_2O_3. The SRO buffer layer was first *in situ* deposited on the quartz substrate at the substrate temperatures of 680 °C, and then the BFO thin film was *in situ* deposited on the SRO/quartz substrate at the substrate temperature of 600 °C. They were deposited under a rf power of 130 W, at a base pressure of 10^{-6} Torr and a deposition pressure of 10 mTorr with Ar and O_2 at a ratio of 4:1. The growth rate of the BFO thin film and SRO buffer layer was about 2.1 and 1.5 nm per minute, respectively. The thickness of the BFO thin film and SRO buffer layer was controlled at ~260 and ~90 nm, respectively. Circular top Au electrodes of 0.1 mm in diameter were sputtered on the film surface using a shadow mask in order to investigate the electrical behavior of the BFO thin film.

The phases present in and the film texture were analyzed by using X-ray diffraction (XRD) (Bruker D8 Advanced XRD, Bruker AXS Inc., Madison, WI, Cu Kα). Field emission scanning electron microscopy (FE-SEM) (Philips, XL30) was employed to study the cross-section and surface morphology of the BFO thin film. Magnetic behavior of the BFO thin film was characterized by using Superconducting Quantum Interference Devices (SQUID, MPMS, XL-5AC, San Diego, CA). Their ferroelectric and leakage behavior were studied by using the Radiant precise workstation (Radiant Technologies, Medina, NY) and a Keithley meter (Keithley 6430, Cleveland, OH). An impedance analyzer (Solartron Grain Phase Analyzer) was used to characterize the dielectric and impedance behavior.

* Corresponding author.
E-mail addresses: msewj@nus.edu.sg, wujiagang0208@163.com (J. Wu), msewangj@nus.edu.sg (J. Wang).

0925-8388/$ – see front matter © 2010 Elsevier B.V. All rights reserved.
doi:10.1016/j.jallcom.2010.07.134

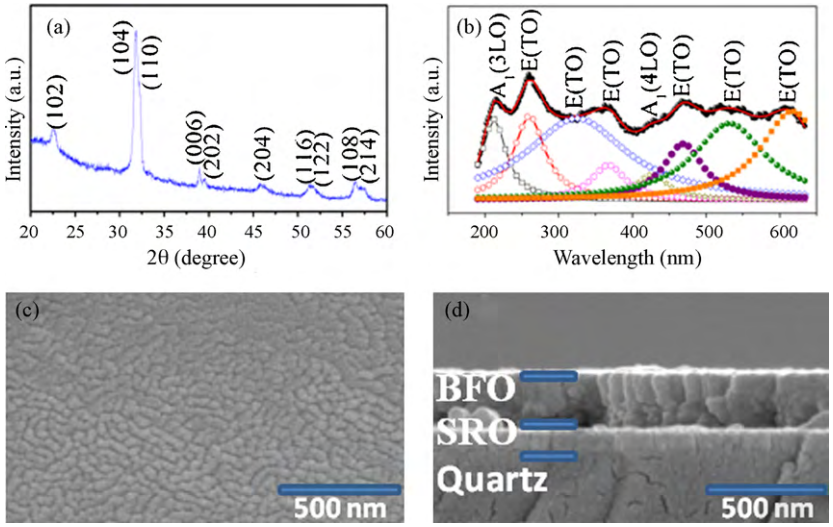

Fig. 1. (a) XRD pattern, (b) Raman spectra, (c) surface morphology, and (d) cross-section for the BFO thin film.

3. Results and discussion

Fig. 1(a) shows the XRD pattern of the BFO thin film deposited on the quartz substrate with a SRO buffer layer. The BFO thin film has a well crystallized perovskite phase structure with random orientation. Fig. 1(b) shows the Raman spectra for the BFO thin film. The *A*1 and *E*-symmetry normal modes for *R*3*c* symmetry could be clearly observed in the wavelength range investigated, which is in agreement with the Raman active vibrational modes of BFO (*R*3*c*) reported [15], confirming that the BFO thin film is of a rhombohedral crystalline structure. Fig. 1(c) and (d) shows the surface morphology and cross-section for the BFO thin film. The thicknesses of BFO and SRO layers were ~260 and ~90 nm, respectively, where the film grains appear to be equiaxed. The film surface morphology and cross-section appear to be dense, crack-free, and well adhered on the SRO buffer layer and the quartz substrate.

Fig. 2(a) plots *P*–*E* loops of the BFO thin film measured at room temperature and 5 kHz. It exhibits a well established hysteresis loop, where its $2P_r$ value is higher than those of BFO thin films [10–12]. To better understand the switchable polarization behavior of the BFO thin film, the pulsed polarization positive up negative down (PUND) measurement was performed at a pulse width of 0.2 ms and room temperature, which was plotted in Fig. 2(b). The polarization value measured by PUND is slightly reduced as compared to that measured by *P*–*E* loops [Fig. 2(a)], confirming that the electrical leakage does not play a big part in the ferroelectric behavior. Fig. 2(c) plots the frequency dependence of the relative permittivity (ε_r) and loss tangent ($\tan\delta$) for the BFO thin film, which shows the ε_r and $\tan\delta$ values of 109 and 3.78% at 10 kHz, respectively. The low $\tan\delta$ values for the BFO thin film indicates that the dielectric behavior is related to the low movable charge density, which is confirmed by the low leakage current in the insert of Fig. 2(c) [16]. The low leakage current is a contributing param-

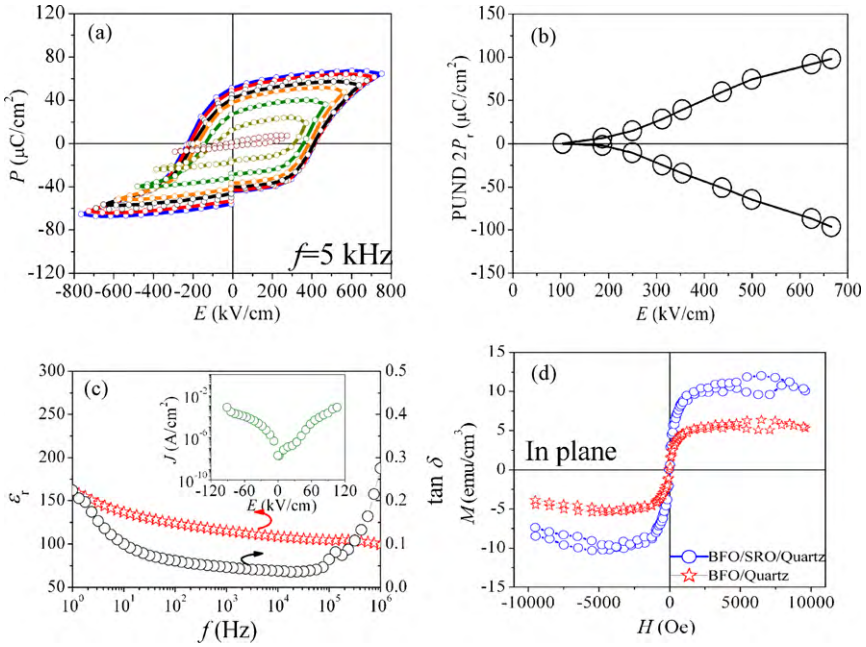

Fig. 2. (a) Ferroelectric behavior, (b) PUND curve, (c) dielectric behavior, and (d) magnetic behavior of the BFO thin film, where the insert in (c) is the curve of *J* vs. *E* for the BFO thin film.

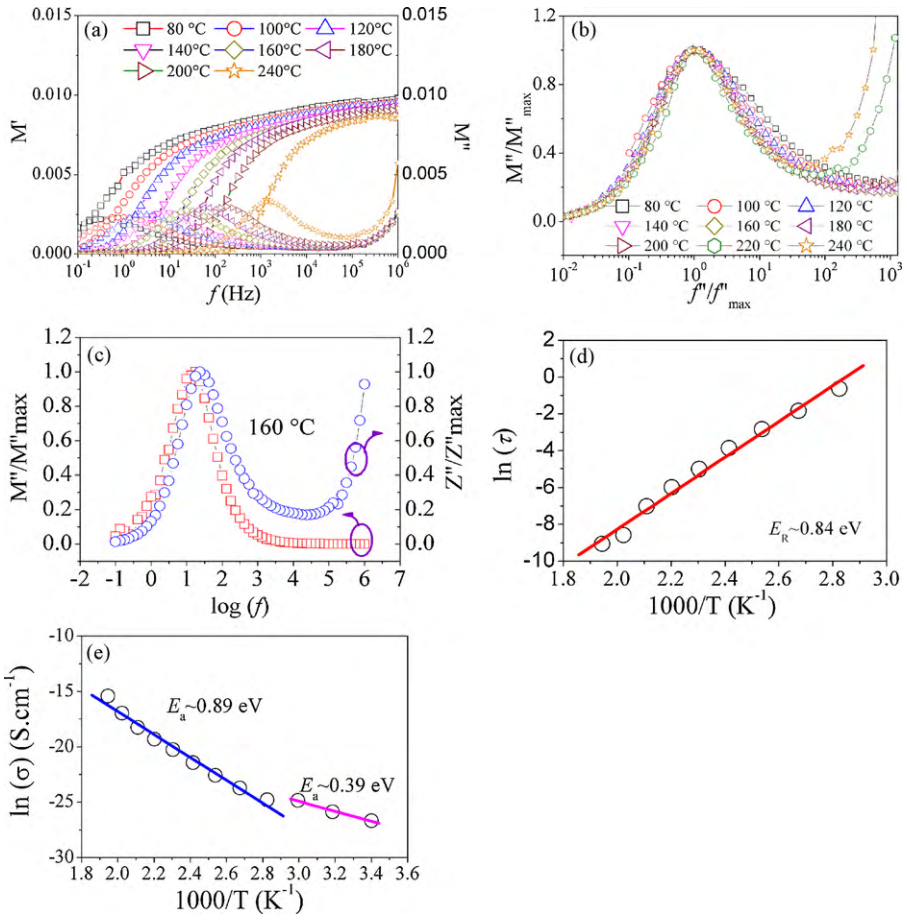

Fig. 3. (a) Complex modulus and master loss, (b) scaling behavior of master spectra, (c) frequency dependence of normalized Z''/Z''_{max} and M''/M''_{max} peaks, (d) relaxation time vs. 1000/T plots, and (e) dc conductivity vs. 1000/T for the BFO thin film.

eter for its large polarization value. Magnetization measurement on the BFO thin film deposited on the SRO/quartz and quartz substrates was conducted at room temperature, the result of which is plotted in Fig. 2(d), where a weakly saturated magnetic loop ($2M_s \sim 10.3$ emu/cm^3) is shown for BFO/quartz.

The electric modulus data are often useful for understanding the different relaxations [17], and the real and imaginary (M' and M'') parts of electrical modulus of BFO thin film as a function of frequencies at different temperatures are shown in Fig. 3(a). The peak position of relaxation frequency is gradually shifted towards higher frequencies with increasing temperature, indicating that the relaxation rate for the process increases with increasing temperature [18]. An increase in temperature leads to a decrease of the value of M' in the low frequency range, but stays almost unchanged at higher frequencies. The scaling behavior of the imaginary part of electric modulus is shown in Fig. 3(b), representing the scaling behavior at different temperatures. They could be largely scaled in a single master curve for electric modulus, suggesting similar thermal activation energy within the sample over the temperature range investigated. Fig. 3(c) shows the frequency dependence of normalized Z''/Z''_{max} and M''/M''_{max} peaks. The peak positions for Z''/Z''_{max} and M''/M''_{max} do not overlap but are very close to each other, indicating a mixture of localized and long-range relaxations [19].

In accordance to the inverse of the maximum frequency peak position in imaginary (M'') of electrical modulus, i.e., $\tau_m = 1/\omega_m$, the temperature dependence of the characteristic relaxation time was determined and plotted in Fig. 3(d), which follows the Arrhenius law $\tau = \tau_o \exp(E_R/k_BT)$ [18]. From the fitting, the value of activation energy is calculated to be ~0.84 eV. Oxygen vacancies ($V_O^{\bullet\bullet}$) are therefore the very likely mobile charges, which often play an important role in the dielectric relaxation for BFO thin films [20]. The calculated value of activation energy suggests that the involvement of oxygen vacancies, where the short-range motion of $V_O^{\bullet\bullet}$ is responsible for the dielectric relaxation in the BFO thin film deposited on the SRO/quartz substrate [21]. The temperature dependence of σ_{dc} can be described by the equation of $\sigma_{dc} = \sigma_{dc0}\exp(-E_a/k_BT)$, where σ_{dc0} is the pre-exponential factor, E_a is the activation energy of dc charge carriers, and k_B is the Boltzmann constant. In Fig. 3(e), the $\ln\sigma_{dc}$ is plotted as a function of reciprocal temperature, where two linear segments of different slopes can be identified, at high and low temperatures respectively. The two E_a values, determined from the slopes of the two linear fragments, are 0.89 eV at $T > 374$ K and 0.39 eV at $T < 374$ K, respectively. The variation in E_a values with increasing temperature suggests that the conductivity process is changed with temperature. At $T < 374$ K, the $E_a \sim 0.39$ eV value indicates that the first-ionization of oxygen vacancies is responsible for conduction [19,21]. At $T > 374$ K, it is likely that the short-range motions ($E_a \sim 0.89$ eV) of $V_O^{\bullet\bullet}$ give rise to electrical conduction [19,21]. The calculated value of E_R is also close to that of E_a at high temperatures, confirming that the same type of charge carriers is responsible for both dielectric relaxation and conduction.

4. Summary

Multiferroic $BiFeO_3$ thin film was grown on the $SrRuO_3$-buffered quartz substrate by off-axis radio frequency magnetron sputtering. The good multiferroic behavior ($2P_r \sim 97.41$ μC/cm^2 and

$2M_s \sim 10.3\,\mathrm{emu/cm^3}$) were obtained for the BFO thin film. On the basis of the temperature- and frequency-dependent impedances, oxygen vacancies are shown to be involved into the dielectric relaxation and electrical conduction of the $BiFeO_3$ thin film, where the scaling behavior of the imaginary part of electric modulus suggests that dielectric relaxation is independent of temperature.

Acknowledgements

Dr. Jiagang Wu gratefully acknowledges the supports of the Singapore Millennium Foundation, the National University of Singapore and the Science and Engineering Research Council (A*Star, Singapore).

References

[1] R. Ramesh, N. Spaldin, Nat. Mater. 6 (2007) 21.
[2] G. Catalan, J.F. Scott, Adv. Mater. 21 (2009) 2463.
[3] L.W. Martin, Y.H. Chu, R. Ramesh, Mater. Sci. Eng. R 68 (2010) 89.
[4] J. Wang, J.B. Neaton, H. Zheng, V. Nagarajan, S.B. Ogale, B. Liu, D. Viehland, V. Vaithyanathan, D.G. Schlom, U.V. Waghmare, N.A. Spaldin, K.M. Rabe, M. Wuttig, R. Ramesh, Science 299 (2003) 1719.
[5] H.W. Jang, D. Ortiz, S.H. Baek, C.M. Folkman, R.R. Das, P. Shafer, Y. Chen, C.T. Nelson, X. Pan, R. Ramesh, C.B. Eom, Adv. Mater. 21 (2009) 817.
[6] J.G. Wu, J. Wang, J. Appl. Phys. 106 (2009) 054115.
[7] H. Béa, M. Bibes, S. Fusil, K. Bouzehouane, E. Jacquet, K. Rode, P. Bencok, A. Barthélémy, Phys. Rev. B 74 (2006), 020101 (R).
[8] H.R. Liu, X.Z. Wang, J. Alloy. Compd. 485 (2009) 769.
[9] J.G. Wu, J. Wang, Acta Mater. 58 (2010) 1688.
[10] H. Zhao, H. Kimura, Z. Cheng, X. Wang, T. Nishida, Appl. Phys. Lett. 95 (2009) 232904.
[11] J.G. Wu, G.Q. Kang, H.J. Liu, J. Wang, Appl. Phys. Lett. 94 (2009) 172906.
[12] J.G. Wu, G.Q. Kang, J. Wang, Appl. Phys. Lett. 95 (2009) 192901.
[13] S. Nakashima, D. Ricinschi, J.M. Park, T. Kanashima, H. Fujisawa, M. Shimizu, M. Okuyama, J. Appl. Phys. 105 (2009) 061617.
[14] A.Z. Simões, R.F. Pianno, E.C. Aguiar, E. Longo, J.A. Varela, J. Alloy. Compd. 479 (2009) 274.
[15] M.K. Singh, H.M. Jang, S. Ryu, M.H. Jo, Appl. Phys. Lett. 88 (2006) 042907.
[16] Z. Cheng, X. Wang, S. Dou, H. Kimura, K. Ozawa, Phys. Rev. B 77 (2008) 092101.
[17] F.D. Morrison, D.C. Sinclair, A.R. West, J. Am. Ceram. Soc. 84 (2001) 531.
[18] A.R. James, S. Priya, K. Uchino, K. Srinivas, J. Appl. Phys. 90 (2001) 3504.
[19] R. Gerhardt, J. Phys. Chem. Solids 55 (1994) 1491.
[20] J.G. Wu, J. Wang, J. Appl. Phys. 105 (2009) 124107.
[21] C. Ang, Z. Yu, L.E. Cross, Phys. Rev. B 62 (2000) 228.